

A 39-Yr Survey of Cloud Changes from Land Stations Worldwide 1971–2009: Long-Term Trends, Relation to Aerosols, and Expansion of the Tropical Belt

RYAN EASTMAN AND STEPHEN G. WARREN

Department of Atmospheric Sciences, University of Washington, Seattle, Washington

(Manuscript received 17 May 2012, in final form 2 August 2012)

ABSTRACT

An archive of land-based, surface-observed cloud reports has been updated and now spans 39 years from 1971 through 2009. Cloud-type information at weather stations is available in individual reports or in long-term, seasonal, and monthly averages. A shift to a new data source and the automation of cloud reporting in some countries has reduced the number of available stations; however, this dataset still represents most of the global land area.

Global-average trends of cloud cover suggest a small decline in total cloud cover, on the order of 0.4% per decade. Declining clouds in middle latitudes at high and middle levels appear responsible for this trend. An analysis of zonal cloud cover changes suggests poleward shifts of the jet streams in both hemispheres. The observed displacement agrees with other studies.

Changes seen in cloud types associated with the Indian monsoon are consistent with previous work suggesting that increased pollution (black carbon) may be affecting monsoonal precipitation, causing drought in northern India. A similar analysis over northern China does not show an obvious aerosol connection.

Past reports claiming a shift from stratiform to cumuliform cloud types over Russia were apparently partially based on spurious data. When the faulty stations are removed, a trade-off of stratiform and cumuliform cloud cover is still observed, but muted, over much of northern Eurasia.

1. Introduction

Climate observations and models suggest that cloud properties have changed and will continue to change in a warming climate. Changes are likely to be seen in cloud amount, height, thickness, geographical distribution, and morphology. Widening tropical belts and warming polar regions may be causing a poleward displacement of the earth's jet streams (Bengtsson et al. 2006; Yin 2005), and cloud-cover distributions are likely to change with a shift in the location of the mean storm track. Greenhouse gases and aerosols can act to alter the lapse rate in the troposphere by either absorbing or scattering radiation (Bollasina et al. 2011; Ramanathan et al. 2005; Menon et al. 2002). Changes in tropospheric stability will also affect cloud amount and type. These and other influences on clouds are investigated here for the land areas of the earth using an updated dataset of visual cloud observations.

Cloud climatologies can be derived from both surface (visual) and satellite observations, and each has its advantages and drawbacks. Some advantages of the surface observations are a long period of record and the ability to identify clouds by type; a disadvantage is incomplete geographical coverage of the globe. The duration and consistency of surface-observed cloud cover allows for the study of trends provided the cloud observations have been subjected to thorough quality control procedures. However, subtle shifts in observing procedure can induce spurious trends into the data record that show up in analyses of ship reports (Bajuk and Leovy 1998; Norris 1999; Eastman et al. 2011), and geopolitical changes can affect the continuity of the record.

In our previous work analyzing cloud cover over land (Warren et al. 2007) we set forth criteria for the examination of surface observations for trends and interannual variations of cloud cover. That work concluded that total cloud cover was declining slightly over the global land areas and hinted that cumuliform clouds may be increasing at the expense of stratiform clouds at low and middle levels. High cloud amount was also

Corresponding author address: Ryan Eastman, Department of Atmospheric Sciences, University of Washington, Box 351640, Seattle, WA 98195-1640.
E-mail: rmeast@atmos.washington.edu

shown to be decreasing. Dim et al. (2011, hereafter D11) compared two satellite datasets [Advanced Very High Resolution Radiometer (AVHRR) and International Satellite Cloud Climatology Project (ISCCP)] and also found a decrease in cloud cover over land, although the character of the change was different in the satellite data—the observed decline was mainly caused by a decrease in low cloud cover. The period of record of these two studies varied by 10 yr (the surface observations being earlier), so exact agreement is not expected, but the attributions of the trends to either high or low clouds are in conflict with each other. Trenberth and Fasullo (2009, hereafter TF09) examined numerous models from phase 3 of the Coupled Model Intercomparison Project (CMIP3) that predict substantial cloud changes within 100 yr. Changes predicted by 2012 are very modest, with only slight increases predicted in middle and high clouds near the poles and declines in low and middle clouds in the midlatitudes. The goal of this study is to use an updated version of our surface-observed dataset to assess these trends and predictions and to explore some examples of the interactions of cloud cover with a changing climate. This updated dataset was already used in a limited-area study of changes in Arctic clouds in relation to sea ice (Eastman and Warren 2010b,a)

2. Data

a. General procedures

Data for this study come from trained human observers at weather stations worldwide. The observations were all reported in the synoptic code of the World Meteorological Organization (WMO 1974). These observations have been archived in many datasets in various countries. The archives that we have been using are the Fleet Numerical Oceanography Center (FNOC, 1971–76), the National Centers for Environmental Prediction (NCEP, 1977–96), and the Integrated Surface Database (ISD) (Smith et al. 2011) at the National Climatic Data Center (NCDC, 1997–2009).

The number of available stations per year has decreased over time (Fig. 1a). The stations shown in this plot represent the subset of 5388 stations chosen by Warren et al. (2007) to form cloud-cover averages; they were chosen because they had long periods of record with cloud-type information. Especially prominent is a decrease in the mid-1990s, which coincides with the automation of weather stations in the United States and Canada. Dai et al. (2006) showed that these automated cloud reports are not compatible with their human-observed predecessors. Also, small-scale compatibility

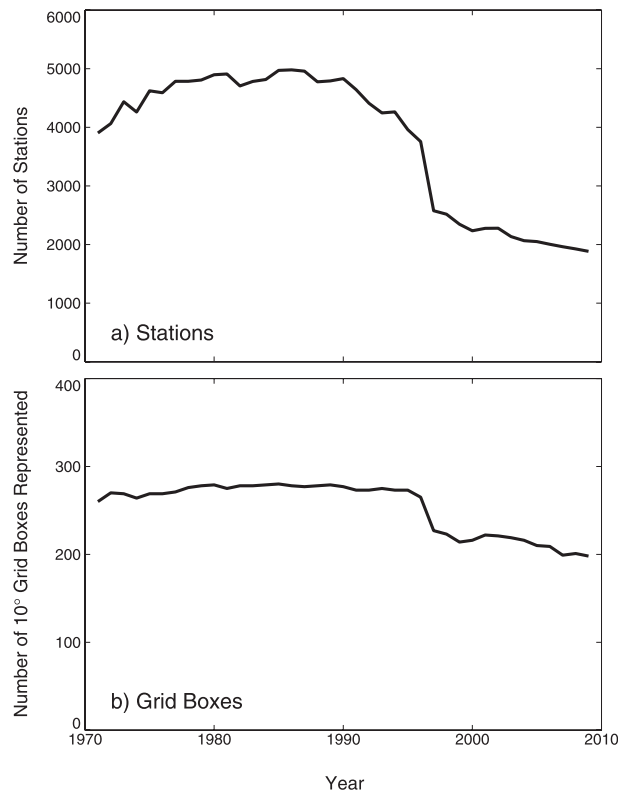


FIG. 1. (a) Number of weather stations with at least 20 observations during July of each year, and (b) the number of 10° equal-area grid boxes represented by the stations present in (a).

issues between the original Extended Edited Cloud Reports Archive (EECRA) and the ISD have caused us to reject some weather stations, enhancing the decline in 1997. Figure 1b shows the number of grid boxes that are occupied by available stations in each year. These boxes are “equal area” boxes measuring 10° of latitude and longitude from 50°S to 50°N , but beyond 50° latitude the longitude bounds increase toward the poles to keep the actual area within the boxes approximately equal, as shown in the maps below. Figure 1b demonstrates that, while available stations have reduced in number, the global coverage of our dataset suffered proportionately less.

The weather stations used in this study were selected as stations that consistently reported cloud types at regular intervals over our period of record. Details concerning this screening are discussed in Warren et al. (2007). Weather reports from these stations are filtered to ensure homogeneous (directly compatible/comparable) cloud data. Each cloud report is interpreted to provide inferred information about precipitating cloud types, fog (not specifically reported as a cloud in the synoptic code, but as present weather), and upper-level clouds. Our

processed reports from these weather stations and from ships together form the Extended Edited Cloud Reports Archive (Hahn et al. 2009), which is available online at the Carbon Dioxide Information Analysis Center web site (<http://cdiac.ornl.gov/epubs/ndp/ndp026c/ndp026c.html>).

Cloud amounts in the EECRA are stored in the WMO format as oktas, or eighths, which represent the fraction of cloud coverage of the sky hemisphere seen by the observer. Clouds are reported at three levels—low, middle, and high—with nine possible cloud types at each level. A random-overlap assumption is applied to middle and high clouds to infer the amount of cloud hidden behind lower clouds. Amounts of middle and high clouds are not computed if they are obscured by lower cloud decks of 6/8 or greater cloud amount because the random-overlap equation becomes inaccurate in those cases. Further details are given by Warren et al. (2007).

Reports are made at 3-h or 6-h intervals at UTC hours divisible by 3. Nighttime observations are scrutinized to ensure adequate illumination, using a criterion established by Hahn et al. (1995). An illuminance indicator in the record is given a value of 0 (not adequate light) if the available light does not meet the criterion, which is equivalent to that of a half-moon at zenith. This calculation is based on a combination of residual sunlight, lunar elevation, and lunar phase. Well-illuminated nighttime observations comprise roughly 30% of available observations. Owing to the possible effects of diurnal cloud cover changes and uneven day–night sampling, we have restricted our analysis in this paper to daytime observations (defined as being taken between 0600 and 1800 local time). However, Warren et al. (2007) showed that in most regions nighttime trends in cloud cover usually agreed with daytime trends.

EECRA reports were averaged at each of the 5388 chosen stations over monthly and seasonal time spans for each year from 1971 through 2009. Long-term seasonal and monthly averages for the span 1971 to 1996 were previously computed and archived by Hahn et al. (2003; available online at <http://cdiac.ornl.gov/epubs/ndp/ndp026d/ndp026d.html>). Files containing average cloud amount, cloud frequency, and amount when present are available. Average amounts were calculated by multiplying the frequency of a cloud type by its amount when present over a specified duration. The original 27 cloud types have been grouped into nine groups: five low [stratus (St), stratocumulus (Sc), fog, cumulus (Cu), and cumulonimbus (Cb)], three middle [nimbostratus (Ns), altostratus (As), and altocumulus (Ac)], and one high-cloud (cirriform) type. Averages of total cloud cover and the frequency of clear sky are also available. This grouping of types was necessary to

TABLE 1. Global-average amounts of cloud types and average cloud-base heights over land and ocean from surface observations. This is an update of Table 2 from Warren et al. (2007). For amounts: Land values are for the period 1971–2009; ocean values are for 1954–2008. For base heights: Land values are for 1971–96, ocean for 1954–97.

Cloud type	Annual average amount (%)		Base height (meters above surface)	
	Land	Ocean	Land	Ocean
Fog	1	1	0	0
Stratus (St)	5	13	500	400
Stratocumulus (Sc)	12	22	1000	600
Cumulus (Cu)	5	13	1100	600
Cumulonimbus (Cb)	5	6	1000	500
Nimbostratus (Ns)	4	5		
Altostratus (As)	4	6		
Altocumulus (Ac)	17	18		
High (cirriform)	22	12		
Total cloud cover	54	68		
Clear sky (frequency)	20	3		

ensure that cloud types were consistent between countries. Table 1 shows global average amounts of these nine cloud types over land (spanning 1971–2009) as well as over the ocean (spanning 1954–2008). Average low-cloud base heights are also shown, although they were not updated over land past 1996 because they were infrequently included in the ISD. To reduce diurnal bias we have selected only report times from the ISD that were used in the original EECRA to make station averages. More detailed information on our filtering and averaging processes are contained in Warren et al. (1986), Warren and Hahn (2002), and the 2012 updates of Hahn et al. (2003) and Hahn et al. (2009).

For a particular year at a station to be used in trend analysis, we require a minimum of 75 daytime observations during each season, or 25 for each month analyzed. In Warren et al. (2007) we computed trends for a station if it had at least 15 yr of data, spanning at least 20 yr; this combination of criteria represented a compromise between geographical coverage and accuracy of trends. In order for a trend to be calculated using this 14-yr update we have changed our criteria to require a span of 30 yr of data with at least 25 individual years present. Global mean trends represent an area-weighted and land-cover-weighted average of trends in all grid boxes, which are averages of all station trends within each box. When producing time series for regions (continent-wide or smaller) instead of trends for individual stations, we have relaxed our standards: the required number of years per station is reduced to 20 and the minimum number of observations to 50. Yearly values for these time series are produced from yearly station anomalies,

averaged within grid boxes, which are subsequently area-weighted and land-cover-weighted and averaged over the entire region. These averaging techniques are necessary to avoid any bias associated with the uneven distribution of weather stations.

b. Identification of erroneous reports in Russia

In preparation of our databases over the last 30 yr, we have examined data in numerous ways to identify stations making erroneous cloud reports that could bias our averages; these stations are identified and their errors discussed in Warren et al. (1986) and Hahn et al. (2003). Our update of the land-station databases to 2009 uncovered some more problems requiring us to remove some stations from the analyses. By far the most significant problem affected 180 stations in Russia, so we discuss their characteristics in detail here as an example of how spurious data can be identified.

Previous studies of cloud changes in the former Soviet Union (Khlebnikova and Sall 2009; Sun and Groisman 2000) have shown a decline in stratiform cloud cover accompanied by an increase in cumuliform cloud cover, particularly in Russia. Those studies were based on cloud data reported in a nation-specific code, not in the synoptic code, but those stations also sent simultaneous reports in the synoptic code to the WMO, which we have analyzed. We have investigated the reported stratiform–cumuliform trade-off to identify which of the nine low cloud types are responsible.

Area-weighted cloud-cover anomaly time series were computed for a region in inland Eurasia bounded by the latitude extremities of the Russian Federation (between 40° and 80°N, 20°E and 180°). Time series were initially produced for all cloud types. A trade-off was shown between stratiform and cumuliform clouds, specifically between the precipitating forms of these clouds (cumulonimbus and nimbostratus). Figure 2 shows these time series for northern winter, December–February (DJF), indicating a steady increase in Cb and a decrease in Ns.

When these time series were examined more closely and contributing stations were analyzed, a disturbing tendency was observed at some stations. Specifically, there appears to be a steplike trade-off between Cb and Ns at some stations that looks like an artifact. This is shown in Figs. 3a and 3b where time series of cloud cover from a single station are plotted. Figures 3a and 3b show that there is an enormous jump in Cb coinciding with a large, though less substantial, decline in Ns. This pattern was seen at a number of stations (on the order of 15%–20%) in Russia with the jumps occurring at different years in different stations, resulting in the more gradual trends in the regional averages shown in Fig. 2.

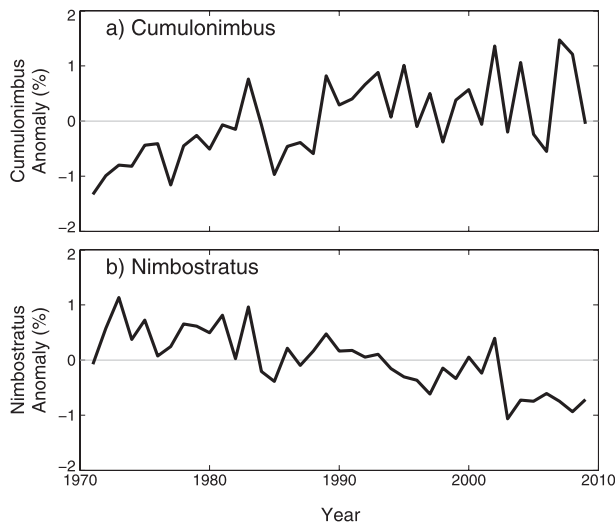


FIG. 2. Cloud cover anomaly time series over Russia and surrounding areas, specifically between 40° and 80°N, 20°E and 180°. Anomalies are calculated for individual stations, then averaged within 10° equal-area grid boxes. Box values are averaged over the entire area, weighted by box size and land fraction.

There was no obvious change in the numbers of observations during the observed jump.

The observed jump in cumulonimbus was tested in two ways to see if it was physical or spurious. The first test is shown in the lower two panels of Fig. 3, which plot cumulus and high clouds at the same station. We expect that, if there was a true substantial change from stratiform to convective precipitation, other cloud types would likely show large changes. Thus, both cumulus and high clouds should increase along with cumulonimbus. This is not observed in Fig. 3, where high clouds continue a steady decline and Cu clouds remain scarce. A second test compared time series at two nearby stations in Fig. 4, one showing a dramatic increase in Cb over 15 yr and a corresponding drop in Ns and the other showing steady amounts of these cloud types. From the figure, it is apparent that prior to the 1990s both stations are observing similar cloud cover and their interannual variations are coherent. After 1992 station 27906 shows a remarkable increase in Cb while station 27928 shows a steady or perhaps even lower amount. This peculiar pattern of contrast between neighboring stations turned out to be widespread in Russia.

The dramatic rise in Cb occurs in different years at different stations. The earliest steps were seen around 1984 and the latest were observed around 2002. Some steps also take a few years to happen, while others take place over just 1 yr. This has made detection difficult since any area-weighted time series for the entire region

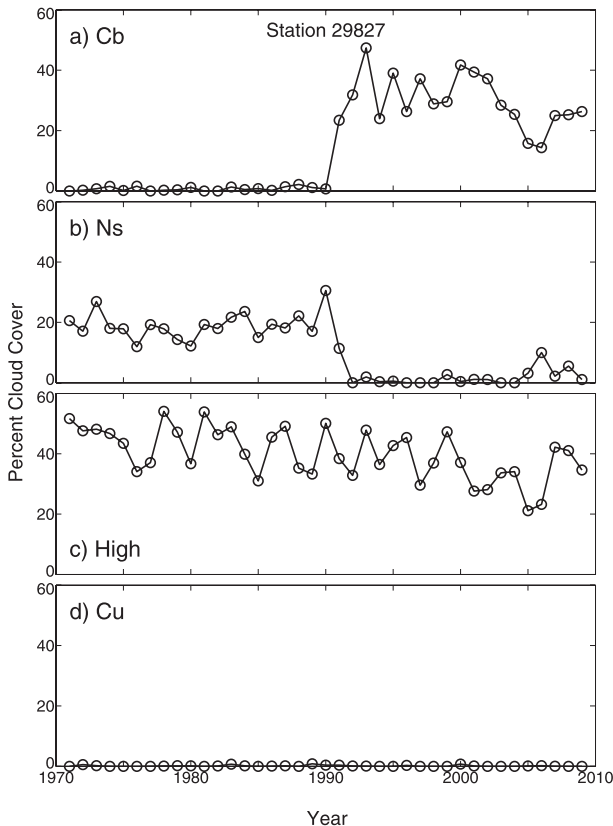


FIG. 3. Time series of (a) cumulonimbus, (b) nimbostratus, (c) high cloud, and (d) cumulus cloud amounts at Russian station 29827 (53.27°N, 80.77°E).

would not show a suspicious steplike increase in cloud amount.

A procedure was designed to find and eliminate problem stations in this region using a step-testing program. Cumulonimbus time series at each station were plotted and fit with a 5-yr running mean. A step was diagnosed where the running mean fit reached its maximum slope. To test whether the step was significant, the mean and standard deviation were calculated before and after the step. If the means before and after the step did not overlap (within their standard deviations), the step was assumed to be significant and the station was flagged. Averages calculated at flagged stations were then removed (given the missing code) from our calculated averages in our updated land climatology for the entire span 1971–2009. This meant a reduction of about 180 stations, which is 15%–20% of the number of Russian stations.

We have not identified the cause for the spurious changes in cloud types shown here. It is most likely the result of an undocumented change in observing procedure or training at some stations. The rejected stations

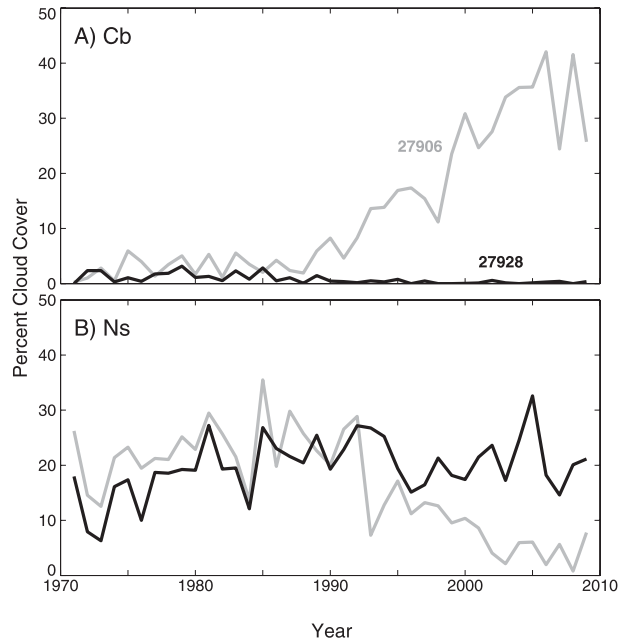


FIG. 4. Time series of (a) cumulonimbus and (b) nimbostratus at neighboring Russian stations 27906 (gray, 53.00°N, 36.03°E) and 27928 (black, 52.63°N, 38.52°E).

do not cluster into an obvious geographic pattern. An examination of the originally reported low cloud values (CL) showed that there was a small shift to more reported CL = 3 and 9 (Cb), versus CL = 4, 5, and 6 (stratiform clouds), which shows a conscious effort to report cumuliform cloudiness, specifically Cb. The present weather code (ww) showed a subtle change between two types of precipitation reported at affected stations. In the early years precipitation was often classified as “slight and steady” snowfall (ww = 71); in later years ww = 71 was less frequent and, instead, “slight and showery snowfall” (ww = 85) was more common.

After these stations were removed from the climatology, the magnitudes of the increase in cumulonimbus and the decrease in nimbostratus over Russia were substantially reduced, though not eliminated. The residual trends could either mean that there are some affected Russian stations with steps that are erroneous, but too small to be rejected by our criterion, or that a real trade-off is also present. We will investigate this further in the next section, looking at Eurasia beyond the boundaries of Russia. The findings of this portion of our study indicate that the observed changes in cloud type over Russia may be unreliable and that corroboration from other climatic variables is needed before an actual trade-off between stratiform and convective precipitation can be concluded. A comparison with the

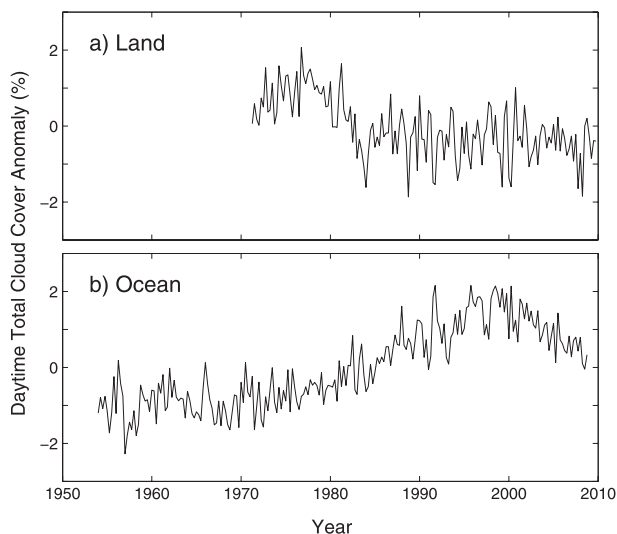


FIG. 5. Global time series of total cloud cover anomalies over land and ocean areas. Each point is a seasonal anomaly. This is an update of Fig. 8 in Eastman et al. (2011). Both time series are based on averages of anomalies in individual 10° grid boxes weighted by land/ocean area and relative box size. Gridbox anomalies over land are based on the average of all station anomalies within each box. Anomalies are defined as the deviation from the long-term mean at a station (land) or a grid box (ocean). No attempt has been made to remove variation from either time series. Owing to changed criteria and the rejection of some weather stations, the plot of land anomalies will not exactly match its previous version in Eastman et al. (2011).

stations used by Sun and Groisman shows that 21 of their 223 stations are among those rejected by our analysis. However, we are unable to say to what extent the Sun and Groisman or Khlebnikova and Sall results are affected by this because they used observations taken in a different code. The database of Hahn et al. (2003) does include these stations but, because that database is of cloud climatologies by station (not by grid box), it is easy for a user to avoid the questionable stations.

3. Global distribution of trends

Shown separately in Fig. 5 are plots of total cloud cover anomalies over global land (with suspicious Russian stations removed) and ocean areas. A similar plot was shown in Eastman et al. (2011) in which the land data terminated at 1996. Long-term variation in the ocean time series was determined to be suspicious, although a direct cause is still unknown. These time series are based on anomalies for individual grid boxes weighted by land/ocean cover and total box area. Further discussion of the methods behind these plots is given in our prior publications. The increase in oceanic cloud cover (which may not be real) shown in Fig. 5b

is offset by a decrease in cloud cover over land up to year 2000, but thereafter the ocean trend reverses. This figure agrees qualitatively with the results of Wylie et al. (2005), who also found little trend in global cloud cover. Although the global time series show little change in total cloud cover, a closer look at cloud types and 10° latitude zones does reveal evidence of changes.

Figure 6 shows trends in yearly-average total cloud cover, stratiform clouds (stratus, stratocumulus, and fog), and cumuliform clouds (cumulus and cumulonimbus) for individual grid boxes. Trends are calculated using the median of pairwise slopes method (Lanzante 1996). These maps are based on data with the aforementioned suspicious Russian stations removed (they are removed for all subsequent analyses in this work). Numbers shown are the average value for all station trends within a grid box in units of $0.1\% \text{ decade}^{-1}$, or percent per century. A station trend is used only if its slope exceeds its standard deviation or the standard deviation is less than $2\% \text{ decade}^{-1}$. In order for a station trend to be included, the record must span at least 30 yr and contain a minimum of 25 data-years per season. The annual-average trend is the mean of the (up to four) seasonal trends. A full set of these trend maps for all cloud types and all seasons is available on our website (www.atmos.washington.edu/CloudMap/LandTrends.html).

Trend values are generally small: most values are around or less than $2\% \text{ decade}^{-1}$. Positive and negative trends occur in cohesive regions that range across international boundaries. Total cloud cover appears to be decreasing over much of the land area except in the Arctic, central northern Africa, and from Indonesia extending into the Pacific islands. South America and Australia show continent-wide decreases in total cloud cover. North America is not well represented owing to the shift away from man-made observations in the United States and Canada.

Even after removal of the suspicious stations in Russia, there appears to be a large-scale trade-off between cumuliform and stratiform clouds over Eurasia. This trade-off spans much of the landmass across many countries but may be reversed in South and Southeast Asia, including India and southern China. A possible mechanism related to atmospheric aerosol may be responsible for this reversal, which is investigated below.

Global average trends are calculated for each plot in Fig. 6. These are calculated using every available grid box, which are area-weighted both by gridbox size and land area. The global averages indicate a decline in total cloud cover over land with a tendency for cumuliform clouds to replace stratiform. Table 2 shows global average trends broken down by season and type. The

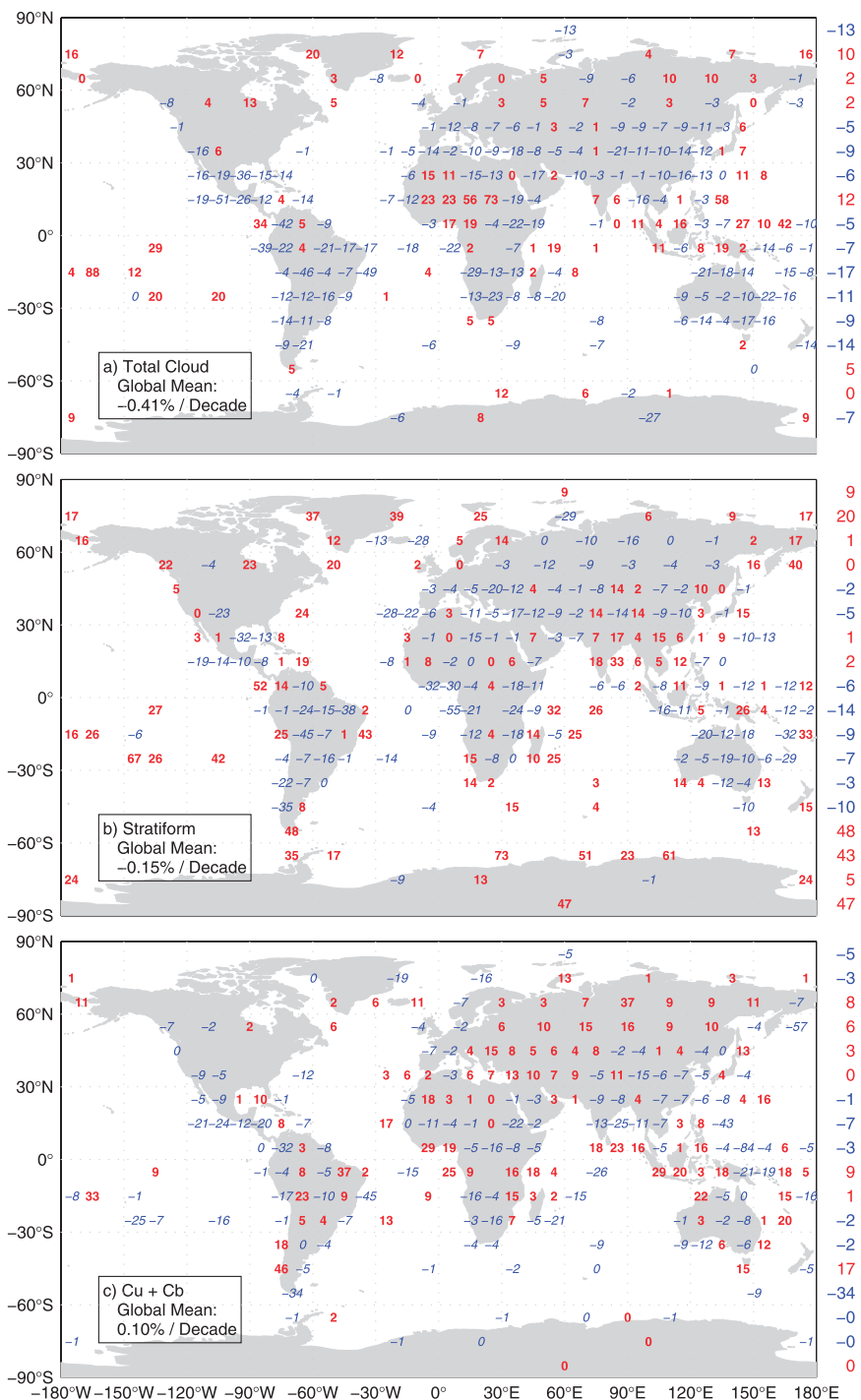


FIG. 6. Annual-average trends for (a) total cloud cover, (b) low stratiform cloud cover (Sc, St, fog), and (c) cumulus cloud cover (Cu, Cb) for the span 1971–2009. Trends are shown for all represented 10° equal-area grid boxes in units of 0.1% decade $^{-1}$. Gridbox averages are based upon the average of all station trends within each box. Zonal averages are shown on the right and represent the mean of all grid boxes in that zone weighted by percent land cover. Global means are shown in percent per decade and represent the mean of all grid boxes weighted by relative area and land fraction. Positive trends are shown bold and in red; negative trends are italicized in blue. A full set of these maps, for all seasons and all cloud types, is made available on our website (www.atmos.washington.edu/CloudMap/LandTrends.html).

TABLE 2. Global trends (percent century⁻¹) for all cloud types for each season and the annual average. Trends are calculated using the same method as in Fig. 6.

Cloud type	DJF	MAM	JJA	SON	Annual
Fog	-0	-0	-1	-0	-0
Stratus (St)	-3	-3	-3	-4	-3
Stratocumulus (Sc)	2	2	2	2	2
Cumulus (Cu)	1	0	1	2	1
Cumulonimbus (Cb)	1	0	0	0	0
Nimbostratus (Ns)	-1	-2	-2	-2	-2
Altostratus (As)	-2	-2	-1	-2	-2
Alto cumulus (Ac)	1	1	0	3	1
High (cirriform)	-1	-7	-2	-3	-2
Total cloud cover	-3	-7	-4	-4	-4
Clear sky (frequency)	1	4	0	2	2

annual average trends are not the arithmetic mean of the global seasonal trends. Instead, they are based on the annual average maps, which may not represent every season in every grid box. Table 2 is an update of Table 3 from Warren et al. (2007). This updated version agrees qualitatively with its older counterpart. The only difference is a reduced magnitude for most trends in the update. This is a likely consequence of the longer time series. Both tables show the tendency for cumuliform to replace stratiform low clouds and both attribute the global reduction in cloud cover mostly to middle and high clouds.

Along the right side of the plots in Fig. 6 are zonal average cloud trends, also in units of 0.1% decade⁻¹. Zonal averages are weighted by the percent of land cover in each box. Figure 7 shows plots of zonal average trends for total cloud cover and for low, middle, and high clouds. Zones containing less than 3% land area (50°–60°S, 80°–90°N) are not included in the plot. Plots in Fig. 7 show small positive or negative trends on the order of 1%–2% decade⁻¹ except in poorly sampled regions in Antarctica. These plots can be compared with those of D11 and with the projections of TF09. D11 compared satellite data from the AVHRR, corrected for orbital drift, and data from the ISCCP, both between 1983 and 2006. TF09 showed predicted cloud cover changes from CMIP3, which compares numerous climate models forced by increasing greenhouse gases from 1970 through year 2100. Both studies show cloud cover trends broken down by latitude and cloud height. Since plots shown in this paper are based solely on land data, exact matching is not expected. A qualitative comparison of these studies is described in Table 3.

In polar regions TF09 project an increase in cloud cover led primarily by middle and high cloud types. Figure 7 shows an increase in clouds at all heights in the Arctic and an increase in low clouds in the Antarctic,

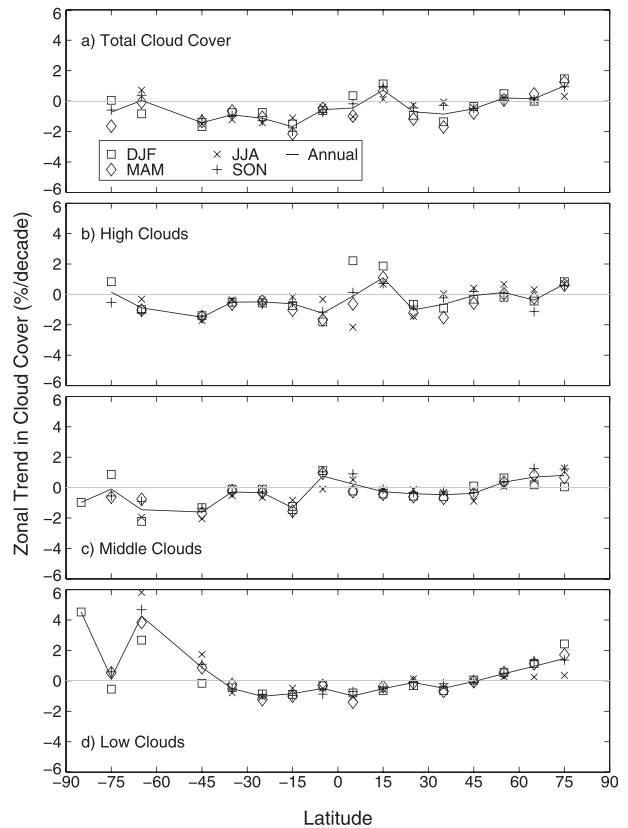


FIG. 7. Seasonal-average and annual-average zonal trends of (a) total cloud cover, (b) high clouds, (c) middle clouds (As, Ac, Ns), and (d) low clouds (fog, Sc, St, Cu, Cb) for 10° latitude bands over 1971–2009. These are calculated using the same method as the zonal trends in Fig. 6. Zones having less than 3% land are not shown.

with near-zero trends of Antarctic middle and high clouds. In D11, Arctic total-cloud-cover trends from satellite data are in opposition, with ISCCP showing an increase led by middle and high clouds, while AVHRR data show a decrease led by middle and low clouds. Both satellite datasets show a decline in the Antarctic, but ISCCP attributes it to low and high clouds whereas AVHRR attributes the decline to middle clouds. Eastman and Warren (2010b) have shown that satellite cloud cover trends over the polar regions can suffer due to issues with cloud detection and possibly orbital drift, while surface observations are lacking in number. This lack of consensus in trends near the poles along with the magnitude of predicted changes highlights the need for further study in these regions.

In middle latitudes (30°–60°), TF09 project a decline in total cloud cover, caused by middle and low clouds. Figure 7 also shows a decline in these regions, but led by declines in middle and high clouds. In Fig. 7 the low clouds appear to be transitioning from positive trends

TABLE 3. A qualitative comparison of TF09, D11, and the updated surface observations in this study. Each region is defined in the left column. A total cloud cover trend is described for each region and dataset, followed by the level most responsible for the trend. A quantitative comparison is not made because of differing time spans and regions. Surface observations over the ocean show spurious variation that makes trend analysis unreliable.

Region	Study		
	Trenberth and Fasullo (2009)(1970–2100, land and ocean)	Dim et al. (2011)(1983–2006, land and ocean)	Updated surface observations (1971–2009, land only)
North, polar north of 60°N	Trend: Increasing contributors, middle and high	Trend–ISCCP: Increasing contributors–middle clouds Trend–AVHRR: Decreasing contributors–middle and low clouds	Trend: Increasing contributors–all levels
North, midlatitude between 30° and 60°N	Trend: Decreasing contributors–middle and low	Trend–ISCCP: Decreasing contributors–low Trend–AVHRR: No trend contributors–offsetting: high increasing, low decreasing	Trend: Decreasing contributors–middle and high
Tropical within 30°N/S	Trend: Decreasing, except at the equator; contributors–middle and high	Trend–ISCCP: Decreasing contributors–low Trend–AVHRR: Increasing contributors–high	Trend: Decreasing, except at 15°N; contributors–low, with mostly decreasing middle, except 10°N–10°S, and decreasing high except 10°–20°N
South, midlatitude between 30° and 60°S	Trend: Decreasing contributors–middle and low	Trend–ISCCP: Decreasing contributors–low Trend–AVHRR: Increasing contributors–high and middle	Trend: Decreasing contributors–middle and high
South, polar south of 60°S	Trend: Increasing contributors–middle and high	Trend–ISCCP: Decreasing contributors–Low and high Trend–AVHRR: Decreasing contributors–middle	Trend–Small decrease Contributors–decreasing middle and high, small increase in low

near the poles to declines closer to the equator. ISCCP trends in D11 show a cloud cover decline in middle latitudes, but the decline is attributed exclusively to low clouds, with middle and high clouds increasing. The AVHRR data show increasing clouds in southern middle latitudes led by high and middle clouds and no trend in northern middle latitudes where increasing high clouds are offsetting decreasing low clouds. In these regions surface observations come closest to agreeing with predicted changes, but significant differences still exist between datasets.

In tropical regions TF09 project declining total cloud cover with no change directly on the equator. Projected declines of middle and high clouds are responsible for this decrease. Figure 7 shows decreasing cloud cover on either side of a lone increasing band centered on 15°N. The land in this zone is mostly in Africa. Middle and high clouds are responsible for this small positive trend, though the increase is farther south for middle clouds. Figure 7 shows low clouds declining in the tropics of both hemispheres. D11 shows disagreement in the satellite datasets, with ISCCP showing a decrease led by low clouds while the AVHRR shows a small increase led by high clouds.

Overall, trends in total cloud cover in Fig. 7 show some similarity to those projected by TF09, with the strongest declines of total cloud cover in middle latitudes and a return to positive or near-neutral trends near the equator and the poles. Comparison with satellite data and at individual levels shows significant spread, however. Some disagreement should be expected given the differing spans and regions sampled, but the extensive qualitative disagreement indicates a lack of consensus on observed cloud changes. Zonal trends in total cloud cover from surface observations over the ocean show a pattern of decline in middle latitudes with very small increases in the tropics and over the Arctic Ocean. We do not include these ocean trends in this analysis since numerous studies (Eastman et al. 2011; Bajuk and Leovy 1998; Norris 1999) have shown that large-scale trends in surface-observed oceanic cloud cover may be spurious.

Figure 8 is an update of Fig. 6 from Warren et al. (2007) showing time series of total cloud cover over all continents except Antarctica, which lacks adequate spatial sampling to produce a reliable time series. The North American time series is shown only prior to 1996 when nearly all weather stations over the United States

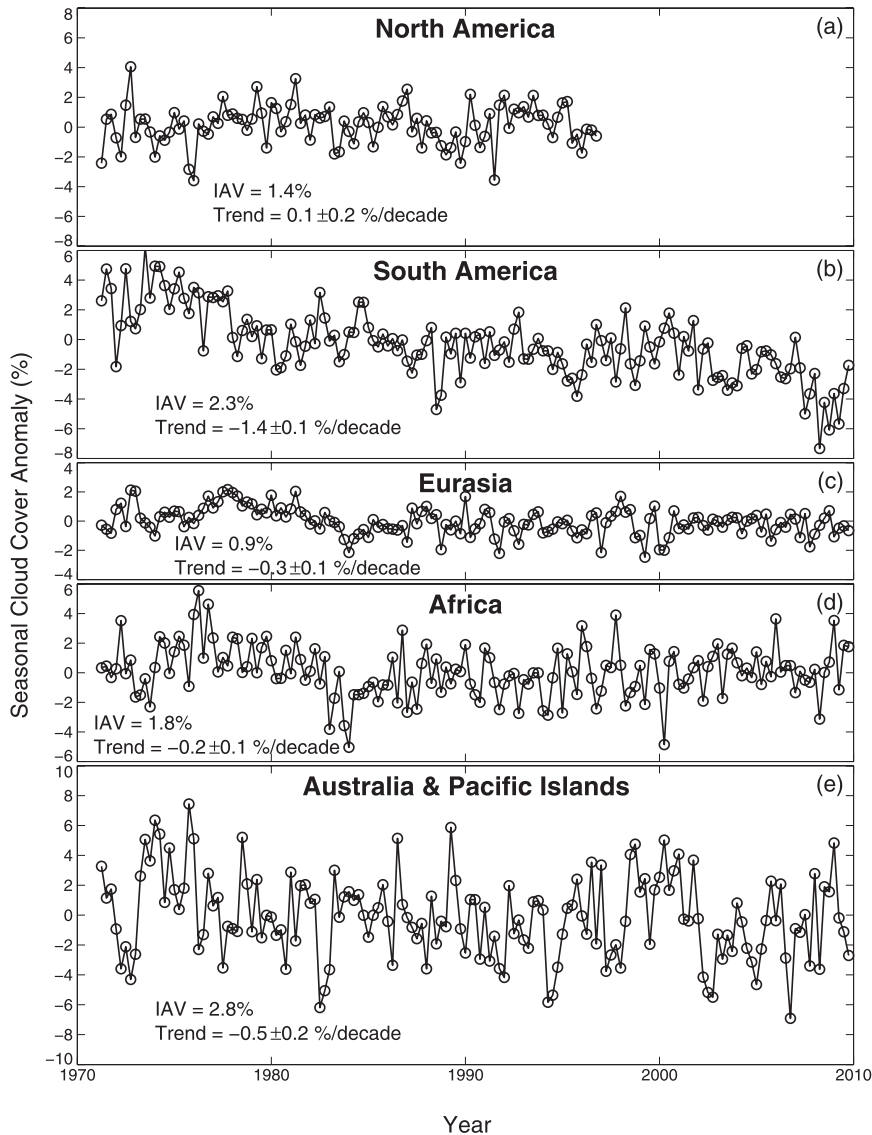


FIG. 8. Seasonal anomaly time series for each continent. Tick marks on the horizontal axis represent DJF. Continental seasonal anomalies are based on seasonal station anomalies averaged within 10° grid boxes, which are then averaged over the continent weighted by land fraction and box size. Interannual variation (IAV) is the standard deviation of the time series. Trends are determined using the “median of pairwise slopes” method.

and Canada switched to automated cloud observations, thus dropping out of our analysis. Time series for the other continents show a continuation of the declining trends shown in the prior paper with little change in interannual variation. South America continues to show the strongest cloud cover reduction, continuing to decline after 1996.

The declining trend in total cloud cover appears widespread over land, encompassing all continents. Middle latitudes show the strongest decreases, and the changes are due to decreases in middle and high clouds, while

low clouds display a subtle trade-off from stratiform to cumuliform clouds. Surface observations over the ocean were also analyzed for trends, but they are not shown because of possible artifacts altering large-scale trends. Using our method of removing these artifacts (detailed in Eastman et al. 2011) the ocean data also suggested declining cloud cover in middle latitudes with positive to near-zero trends in the tropics and over the Arctic. The declines in total cloud cover seen at middle latitudes and the increases in the Arctic agree with recent predictions by global climate models, given greenhouse warming. In

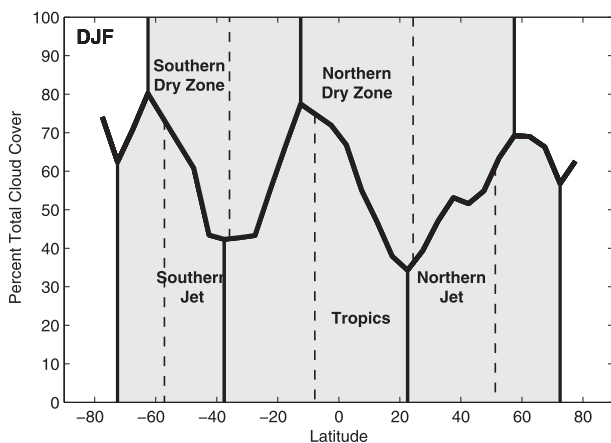


FIG. 9. Total cloud cover vs latitude during DJF. Jet stream (also referred to as the storm track), dry zone, and tropical regions are shown in gray bordered by solid vertical lines. The center of mass for each region is shown as the black dashed vertical line near the middle.

the next section, we will show that these trends may be due to a poleward expansion of the Hadley cell and a subsequent poleward shift in midlatitude jet streams.

4. Expansion of tropical belts and poleward migration of storm tracks

A number of studies have shown a widening of the tropical belt (Seidel et al. 2008; Bender et al. 2011; Hudson et al. 2006) and an accompanying poleward shift in the subtropical jet streams (Archer and Caldeira 2008; Fu and Lin 2011). Here, we use an analysis of the “center of mass” of a 2D plot of cloud cover in latitude bands associated with these regions to see if any significant shifts have occurred since 1971.

Stations selected for this analysis were required to have data for at least 36 of the possible 39 years. A single season of a single year is used if the station has at least 50 observations. Because of the unfortunate transition from human cloud observations to automated systems, this analysis cannot include North America. However, a separate analysis, which includes North American stations through 1994, will be shown below. To avoid biases associated with the uneven distribution of stations, station averages are first averaged within 5° equal-area grid boxes. We use the 5° grid rather than the 10° grid to improve the resolution of our plots. Box averages are then land-area weighted for computation of zonal averages.

Latitude bands representing the midlatitude storm track and the tropical regions for all cloud types are chosen using the distribution of total cloud cover versus latitude. As detailed in Fig. 9, “storm track” regions are identified as the latitude bands poleward of the

subtropical desert regions. Dry zones are shown as the latitude bands between the tropical cloud maximum and the cloud maximum associated with the storm tracks. Latitude bands are determined independently for each season based upon that season’s distribution of total cloud cover. Archer and Caldeira (2008) have shown the existence of multiple storm tracks in the Southern Hemisphere. However, the coarse nature of our data prohibits us from effectively studying multiple storm tracks in each hemisphere, so in the midlatitudes all clouds associated with the storm tracks are lumped into one band. The distribution of cloud types within each band will vary and may not necessarily match that of total cloud cover, but our goal is to discern which types may contribute to changes in the overall pattern.

Our center-of-mass analysis finds the area under a curve using the trapezoidal numerical integration method. The latitude resolution of the cloud amount versus latitude plot is enhanced using linear interpolation between points. The center of mass for each region is then determined using an iterative routine that slices the distribution repeatedly until half of the total “mass” lies on one side of a point along the latitude axis. The center of mass for dry zones uses the area *above* the curve whereas the area *below* the curve is used for cloudy regions. An example is shown in Fig. 9, which shows the long-term mean total cloud cover in DJF. The centers of mass are shown as dashed lines.

To create the time series for each band shown in Fig. 10, seasonal plots of cloud cover versus latitude were analyzed for each year in the manner shown in Fig. 9. The yearly anomaly of the center of mass for each band was calculated as the average of each season’s deviation from its long-term seasonal-mean center of mass. Figure 10 shows this yearly anomaly along with a best-fit line, determined using robust multilinear regression. Best-fit lines are shown in black (or red) if they are 95% significant. Nonsignificant fits are shown in gray.

The time series in Fig. 10 show significant poleward shifts in total cloud cover associated with the Northern and Southern Hemisphere storm tracks. The dry zones also shift poleward, but not significantly. In the tropics there is a relatively strong northward shift of cloud cover. Trend maps (available online) indicate that this northward shift may be due to cloud increases in the Sahel combined with decreases over South America. Numerical values for the linear fits for other cloud types in these bands are shown in Table 4. Changes seen in total cloud cover in storm-track regions and the tropics are supported by observed changes in cloud types. Specifically, precipitating clouds as well as low clouds are moving significantly poleward in both storm-track

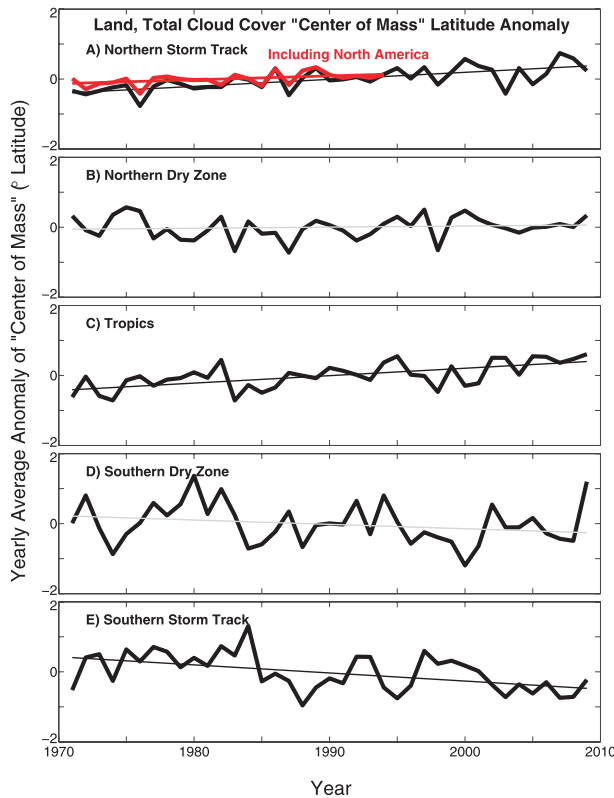


FIG. 10. Yearly average latitudinal anomalies of the center of mass for distributions of cloud cover in each region. Also shown is the best-fit line, calculated using robust multilinear regression. Best-fit lines are black or red if 95% significant and gray if not.

regions and are moving to the north in the tropics. Cumuliform clouds are showing particularly strong, and somewhat alarming, northward trends in all three regions. This necessitates future investigation. In the top panel of Fig. 10 a second plot is shown for a set of stations including North America. Although the poleward shift has a lower magnitude, a significant northward trend is still observed. Dry-zone changes look variable and inconsistent between types.

Storm track shifts may also be related to ENSO. Seager et al. (2005) say that “During El Nino events the jets

strengthen in each hemisphere and shift equatorward” (p. 1501). In Table 5, the seasonal time series used to produce Fig. 10 are correlated with an ENSO index (Meyers et al. 1999). Latitudinal anomalies are kept in units of north–south deviation, so a deviation to the north is positive in both hemispheres. We remove the long-term variation from each time series by subtracting the 5-yr running mean, so only year-to-year variations are compared, unaffected by trends. We do see a consistent pattern supporting the conclusion that positive ENSO events are associated with an equatorward shift in both the Northern and Southern Hemisphere storm tracks. Associated dry zones also show a strong tendency to shift toward the equator during positive ENSO events. Also during positive ENSO, clouds in the tropics show a tendency, although not statistically significant, to shift south during DJF and March–May (MAM) and north during June–August (JJA) and September–November (SON).

This section supports previous conclusions concerning the behavior of the jet streams and the recent trends in the migration of the jet streams. For the storm-track regions, our poleward trend values are within the bounds shown by Fu and Lin (2011), although our values are larger in magnitude than those shown by Archer and Caldeira (2008). A northward shift of the tropical cloud cover distribution is also seen, which was not predicted; it deserves further investigation.

We have also done this analysis globally, using land and ocean data. Ocean data come from synoptic observations made by observers on ships, and these reports are also stored in the EECRA. Seasonal averages of cloud amounts from ship reports are gridded on a 10° latitude/longitude grid and are available as a gridded climatology (Hahn et al. 2007). Spurious variation has been removed and the observations have been processed using the methods in Eastman et al. (2011). Using these ocean gridbox values combined with those over land, we have identified similar bands as in Fig. 9 and plotted time series analogous to Fig. 10. Averages within each 10° latitude band are based on land/ocean area

TABLE 4. Northward trends of the yearly averaged center of mass of the cloud cover distribution in each region for total cloud cover and selected cloud types. Trends are the slope of the best-fit line (as calculated for Fig. 10). Trends significant within 95% confidence bounds are shown in bold.

Region	Trends of center of mass anomalies over land (km decade ⁻¹)						
	Total cloud cover	Precipitating cloud	Low cloud	Cumuliform cloud	Stratiform cloud	Middle cloud	High cloud
Northern storm track	22	20	36	87	29	68	7
Northern dry zone	3	−4	−7	−13	6	−8	−7
Tropics	23	41	29	28	31	6	18
Southern dry zone	−13	−3	28	0	24	−41	−2
Southern storm track	−26	−44	−108	97	−100	−22	−42

TABLE 5. Seasonal time series from Fig. 10 correlated with a seasonal ENSO index (Meyers et al. 1999). Latitudinal anomalies are kept in units of north–south deviation, so a deviation to the north is positive in both hemispheres. We remove long-term variation from each time series by subtracting the 5-yr running mean, so only year-to-year variations are compared. Correlations are shown in bold if significant at the 95% level.

	DJF	MAM	JJA	SON	Yearly
Northern storm track	-0.37	-0.18	-0.40	-0.39	-0.29
Northern dry zone	-0.75	-0.65	-0.30	0.01	-0.48
Tropics	-0.24	-0.18	0.20	0.27	0.07
Southern dry zone	0.32	0.34	0.50	0.44	0.56
Southern storm track	0.34	0.33	0.23	0.52	0.36

weighted averages. The southern storm track represents ocean data only from DJF. Data in other seasons were too sparse to be considered reliable. These time series are shown in Fig. 11, which shows best-fit lines and highlights the seasonal spread of the yearly values. The blue “fill” in each plot shows the range of seasonal anomalies for each year. Figure 11 suggests that storm track changes over the ocean are not as strong as those poleward shifts seen over land, but the poleward migrations in dry regions are enhanced over the ocean. The tropical band shows only a very small northward trend compared to the strong change seen over land alone. Variations within these bands also correlated significantly with the ENSO index, especially in the dry regions. Figure 11 further suggests that expansion of the tropics is significant and ongoing, and not just confined to land areas.

5. Clouds and aerosols in India and China

Droughts have recently been observed in northeast China as well as in northern India. The boundary layer atmosphere in these heavily populated regions has high anthropogenic aerosol content, which in many regions has been increasing. Increased atmospheric aerosols may contribute to patterns of drought through multiple mechanisms (Bollasina et al. 2011; Ramanathan et al. 2005). Pollution with a large amount of black carbon can absorb sunlight in the troposphere while reducing sunlight received at the surface. This has the effect of stabilizing the atmosphere and hindering convection. Also, more numerous cloud condensation nuclei can increase cloud droplet concentrations while reducing droplet size. This reduces precipitation and prolongs the life of clouds. These aerosol effects are likely to produce noticeable changes in cloud type, specifically a decline in cumuliform cloud types accompanying a rise in stratiform clouds. Precipitating clouds, especially cumulonimbus, should decrease with increasing aerosol concentration.

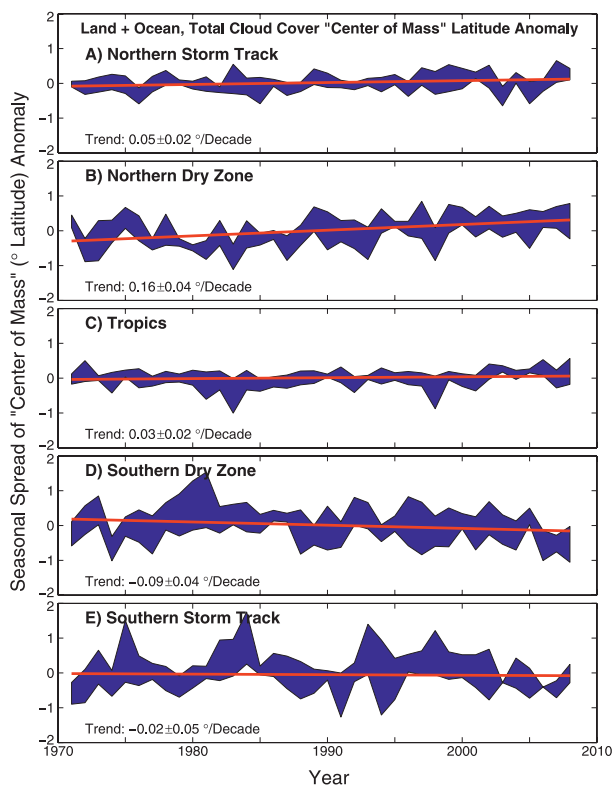


FIG. 11. Seasonal spread of latitudinal anomalies of the center of mass for distributions of cloud cover in each region using data over both land and ocean areas. Also shown is the best-fit line, calculated using robust multilinear regression. Land data are filtered using the same criteria as Fig. 10; ocean grid boxes require at least 35 yr of data over the span 1971–2008, with a minimum of 25 observations per grid box.

Precipitation in South and Southeast Asia is strongly linked to the summer monsoon. Warming of the land-mass relative to the ocean drives a large-scale overturning of the atmosphere, with rising motion and significant precipitation over land areas. Figure 12 shows that the Indian summer monsoon (ISM) index (Wang and Fan 1999; Wang et al. 2001) correlated with total cloud cover during JJA. Aside from the expected positive correlation between the ISM and cloud cover over India, this map also shows the extent to which the ISM is related to variability in cloud cover over the globe. The ISM index correlates significantly with clouds in areas as far away as western North America and southern South America. Given this complex, wide-ranging effect, it is likely that changes in the Indian monsoon can affect climate on a global scale.

A map of trends in precipitating clouds during JJA (not shown) does not mesh well with the dot plot in Fig. 12. Regions of positive and negative trends do not coincide with areas of positive and negative correlation.

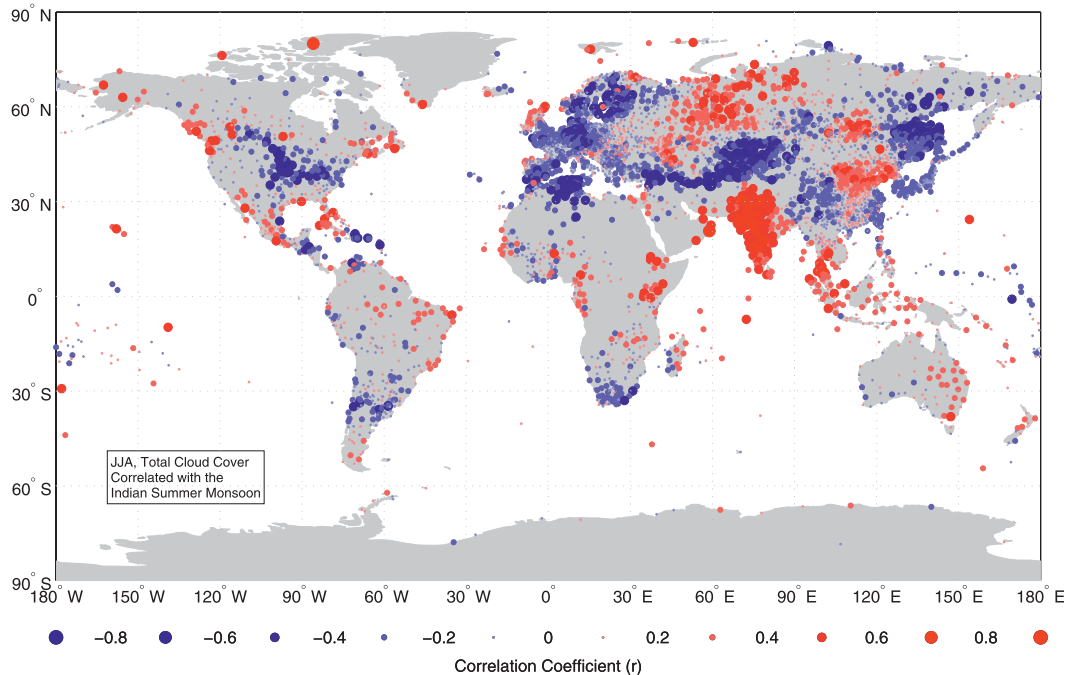


FIG. 12. Total cloud cover anomalies correlated with the Indian summer monsoon index during JJA. Coefficients are shown at each station as dots, with dot size and color relative to correlation strength. Correlation coefficients are plotted if stations have at least 20 yr of cloud data with at least 50 observations per year for that season.

Also, the monsoon index does not show a pronounced trend from 1971 through 2009. Therefore it is unlikely that a wholesale trend in the monsoon index is to blame for the drought in northern India. This leaves the possibility of other localized effects, such as atmospheric aerosols. We split India into two regions for this study. A northern section has the same boundaries as in Bollasina et al. (2011), bounded by 20°–28°N, 76°–87°E. A southern section contains all stations in India south of 20°N. These regions were chosen to contrast the polluted north with the relatively cleaner south.

Figures 13 and 14 show the monthly linear trend of cloud-cover for total, precipitating, cumuliform, stratiform, cumulonimbus, and nimbostratus cloud for northern and southern India. In Fig. 13 (northern India) the predicted cloud response to increasing aerosols is mostly observed. Between July and October there is a decreasing trend in precipitating clouds, especially Cb. Also during that time there is an observed decline in cumuliform clouds. Stratiform clouds are seen to be increasing throughout the year. Shown in Fig. 14, stratiform clouds in the south are also increasing at the expense of cumuliform; however, precipitating clouds are seen to be increasing during the rainy season. Cumulonimbus amounts appear nearly steady, while Ns is shown to be mostly responsible for the increase. These plots suggest that the switch from

cumuliform to stratiform cloud cover is actually occurring over both north and south India, while the predicted precipitation decline is happening mostly in the north.

In northeastern China precipitation trends have been shown to be negative (Gemmer et al. 2004; Zhao et al. 2010) and cloud cover has been decreasing (Endo and Yasunari 2006; Xia 2012; Warren et al. 2007; Kaiser 2000). Xia (2012) showed that the frequency of clear skies has been increasing and, by comparing cloud records in “clean” regions to those in more polluted regions, showed that this increase is not due to thin clouds being obscured by aerosols as suggested by Warren et al. (2007). Upon examination, cloud changes in this region are not consistent with changes caused by an increase in aerosols. Precipitating cloud amount is declining slightly throughout the year, but low cumuliform and low stratiform clouds are declining. Cumulonimbus is increasing during summer, while Ns is decreasing year-round. This is consistent with Lei et al. (2011) and Feng et al. (2011), who see and predict, respectively, an increase in precipitation intensity but a decline in the number of rainy days. In southern China, Endo and Yasunari (2006) have shown a decline in the frequency of Cb, while the amount when present has been rising, suggesting an increase in the intensity of precipitation. Southeast China has not been experiencing

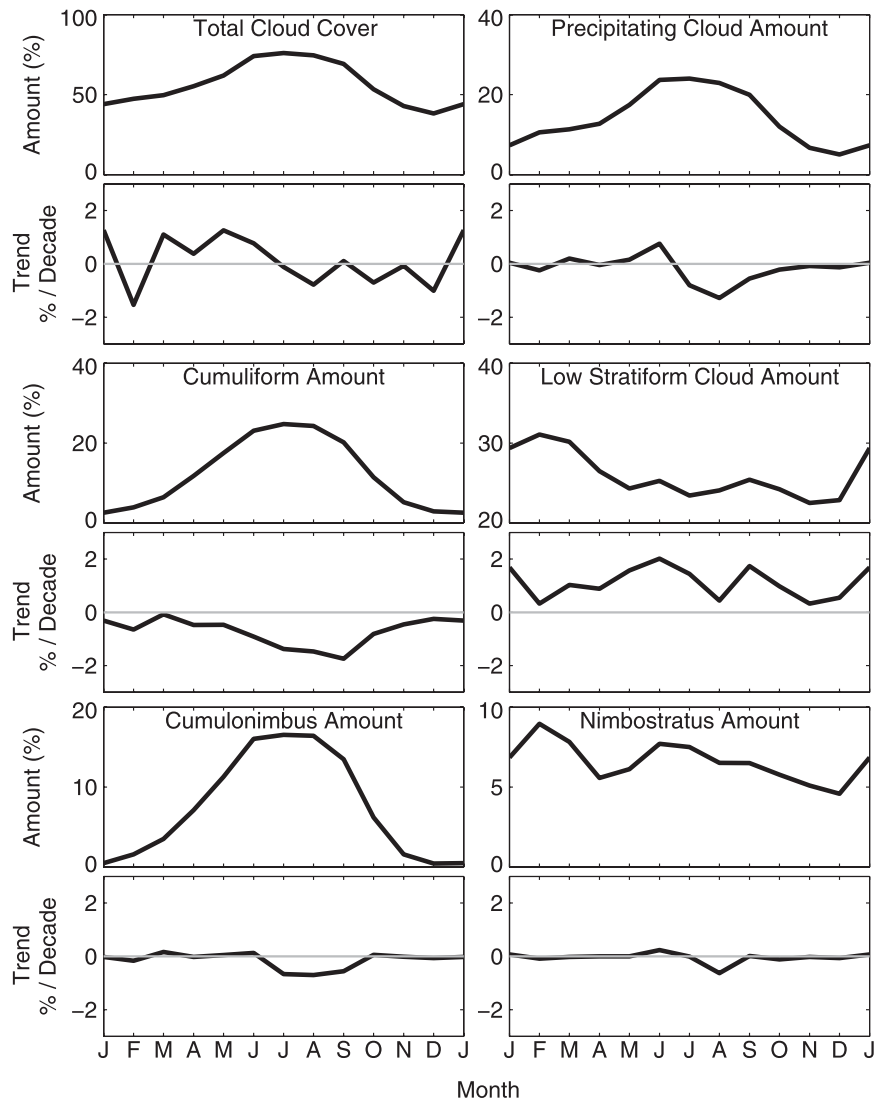


FIG. 13. Monthly trends of total cloud cover, precipitating clouds (Ns, Cb), cumuliiform clouds (Cu, Cb), stratiform clouds (St, Sc, fog), cumulonimbus clouds, and nimbostratus clouds over northern India (20° – 28° N, 76° – 87° E). Trends are calculated using robust multilinear regression.

a drought, although there are cloud changes that may be related to aerosols. During summer cumuliiform clouds are decreasing while stratiform clouds are increasing, a possible result of increased aerosols.

6. Discussion and conclusions

The update in this dataset offers few surprises. Many of the changes seen in Warren et al. (2007) are still taking place now, although the magnitudes of the changes are smaller over the longer time span. Over land, the global total cloud cover record shows a decline during the 1970s and 1980s followed by a steady cloud amount through 2009 with interannual variation

on the order of $\pm 1\%$. The observed decline is due to decreasing clouds at middle and high levels. Middle latitudes are responsible for much of the decline in total cloud cover, which roughly agrees with climate model predictions. Agreement is less apparent when different levels are analyzed, and satellite-based datasets do not show agreement with surface observations, predictions, or each other. The decline in midlatitude clouds is consistent with the observed expansion of the tropics and the poleward migration of the jet streams.

A previously reported trade-off from stratiform to cumuliiform cloud cover over Russia was partly spurious, based on data from bad weather stations. Although

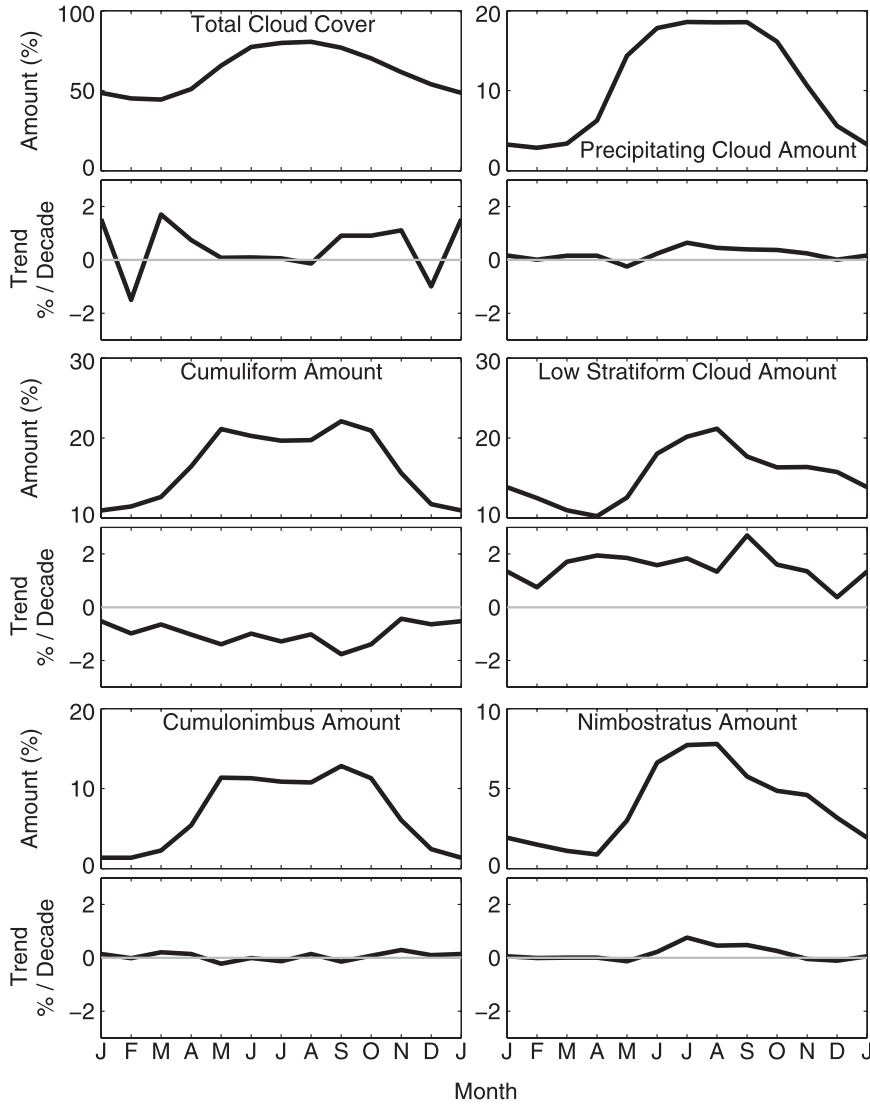


FIG. 14. As in Fig. 13 but over southern India (all stations south of 20°N).

a cause for the unrealistic steplike behavior between stratiform and cumuliform clouds is not known, the magnitude of the jump and lack of corroboration casts doubt on the integrity of these observations. However, even after removal of the questionable stations there is evidence of a tendency for cumulus cloud to increase at the expense of stratiform. This behavior spans much of Eurasia across numerous international boundaries, lending some credibility to its physical existence.

Anthropogenic aerosols may be affecting cloud cover and precipitation associated with the Indian monsoon. Cloud changes in northern India during the monsoon (increasing stratiform, decreasing cumuliform) are consistent with those expected given greater black carbon

in the troposphere. Over northeastern China the cloud changes do not appear to be directly related to aerosols.

Cloud cover will continue to evolve in a changing climate while surface reports of visual observations may continue to decline in number. This study has shown that changes in cloud type at multiple levels may be more substantial and have a greater overall impact than changes in total cloud cover. With the continued automation of cloud observation it will be important either to preserve systems that can accurately see cloud type and height or to develop new forms of detection that take these important cloud properties into account.

Acknowledgments. Carole Hahn scrutinized the ISD as a source dataset to identify problems requiring

attention in the analysis. We thank Robert Wood and Qiang Fu for the helpful discussion. The research was supported by NSF Grant AGS-1021543.

REFERENCES

- Archer, C. L., and K. Caldeira, 2008: Historical trends in the jet streams. *Geophys. Res. Lett.*, **35**, L08803, doi:10.1029/2008GL033614.
- Bajuk, L. J., and C. B. Leovy, 1998: Are there real interdecadal variations in marine low clouds? *J. Climate*, **11**, 2910–2921.
- Bender, F. A.-M., V. Ramanathan, and G. Tselioudis, 2011: Changes in extratropical storm track cloudiness 1983–2008: Observational support for a poleward shift. *Climate Dyn.*, **38**, 2037–2053.
- Bengtsson, L., K. I. Hodges, and E. Roeckner, 2006: Storm tracks and climate change. *J. Climate*, **19**, 3518–3543.
- Bollasina, M. A., Y. Ming, and V. Ramaswamy, 2011: Anthropogenic aerosols and the weakening of the South Asian summer monsoon. *Science*, **334**, 502–505.
- Dai, A., T. R. Karl, B. Sun, and K. E. Trenberth, 2006: Recent trends in cloudiness over the United States: A tale of monitoring inadequacies. *Bull. Amer. Meteor. Soc.*, **87**, 597–606.
- Dim, J. R., H. Murakami, T. Y. Nakajima, B. Nordell, A. K. Heidinger, and T. Takamura, 2011: The recent state of the climate: Driving components of cloud-type variability. *J. Geophys. Res.*, **116**, D11117, doi:10.1029/2010JD014559.
- Eastman, R., and S. G. Warren, 2010a: Arctic cloud changes from surface and satellite observations. *J. Climate*, **23**, 4233–4242.
- , and —, 2010b: Interannual variations of Arctic cloud types in relation to sea ice. *J. Climate*, **23**, 4216–4232.
- , —, and C. J. Hahn, 2011: Variations in cloud cover and cloud types over the ocean from surface observations, 1954–2008. *J. Climate*, **24**, 5914–5934.
- Endo, N., and T. Yasunari, 2006: Changes in low cloudiness over China between 1971 and 1996. *J. Climate*, **19**, 1204–1213.
- Feng, L., T. J. Zhou, B. Wu, T. Li, and J.-J. Luo, 2011: Projection of future precipitation change over China with a high-resolution global atmospheric model. *Adv. Atmos. Sci.*, **28**, 464–476.
- Fu, Q., and P. Lin, 2011: Poleward shift of subtropical jets inferred from satellite-observed lower-stratosphere temperatures. *J. Climate*, **24**, 5597–5603.
- Gemmer, M., S. Becker, and T. Jiang, 2004: Observed monthly precipitation trends in China 1951–2002. *Theor. Appl. Climatol.*, **77**, 39–45.
- Hahn, C. J., S. G. Warren, and J. London, 1995: The effect of moonlight on observation of cloud cover at night, and application to cloud climatology. *J. Climate*, **8**, 1429–1446.
- , —, and R. Eastman, 2003: Cloud climatology for land stations worldwide, 1971–1996. Tech. Rep. NDP-026D, Carbon Dioxide Information Analysis Center, 35 pp. [Available online at <http://cdiac.ornl.gov/ftp/ndp026d/>; associated data files have been updated to 2012.]
- , —, and —, 2007: A gridded climatology of clouds over land (1971–96) and ocean (1954–97) from surface observations worldwide. Carbon Dioxide Information Analysis Center Rep. NDP-026E, 71 pp. [Available online at <http://cdiac.ornl.gov/ftp/ndp026e/>; associated data files have been updated to 2010.]
- , —, and —, 2009: Extended edited synoptic cloud reports from ships and land stations over the globe, 1952–1996 (updated to 2009). Numerical Data Package NDP-026C, Carbon Dioxide Information Analysis Center (CDIAC). [Available online at <http://cdiac.ornl.gov/epubs/ndp/ndp026c/ndp026c.html>; updates to 2012 are available.]
- Hudson, R. D., M. F. Andrade, M. B. Follette, and A. D. Frolov, 2006: The total ozone field separated into meteorological regimes—Part II: Northern Hemisphere mid-latitude total ozone trends. *Atmos. Chem. Phys.*, **6**, 5183–5191.
- Kaiser, D. P., 2000: Decreasing cloudiness over China: An updated analysis examining additional variables. *Geophys. Res. Lett.*, **27**, 2193–2196.
- Khlebnikova, E. I., and I. A. Sall, 2009: Peculiarities of climatic changes in cloud cover over the Russian Federation. *Russ. Meteor. Hydrol.*, **34**, 411–417.
- Lanzante, J. R., 1996: Resistant, robust and non-parametric techniques for the analysis of climate data: Theory and examples, including applications to historical radiosonde station data. *Int. J. Climatol.*, **16**, 1197–1226.
- Lei, Y., B. Hoskins, and J. Slingo, 2011: Exploring the interplay between natural decadal variability and anthropogenic climate change in summer rainfall over China. Part I: Observational evidence. *J. Climate*, **24**, 4584–4599.
- Menon, S., J. Hansen, L. Nazarenko, and Y. Luo, 2002: Climate effects of black carbon aerosols in China and India. *Science*, **297**, 2250–2253.
- Meyers, S. D., J. J. O'Brien, and E. Thelin, 1999: Reconstruction of monthly SST in the tropical Pacific Ocean during 1868–1993 using adaptive climate basis functions. *Mon. Wea. Rev.*, **127**, 1599–1612.
- Norris, J. R., 1999: On trends and possible artifacts in global ocean cloud cover between 1952 and 1995. *J. Climate*, **12**, 1864–1870.
- Ramanathan, V., and Coauthors, 2005: Atmospheric brown clouds: Impacts on South Asian climate and hydrologic cycle. *Proc. Natl. Acad. Sci. USA*, **102**, 5326–5333.
- Seager, R., N. Harnik, W. A. Robinson, Y. Kushnir, M. Ting, H.-P. Huang, and J. Velez, 2005: Mechanisms of ENSO-forcing of hemispherically symmetric precipitation variability. *Quart. J. Roy. Meteor. Soc.*, **131**, 1501–1527.
- Seidel, D. J., Q. Fu, W. J. Randell, and T. J. Reichler, 2008: Widening of the tropical belt in a changing climate. *Nat. Geosci.*, **1**, 21–24.
- Smith, A., N. Lott, and R. Vose, 2011: The integrated surface database: Recent developments and partnerships. *Bull. Amer. Meteor. Soc.*, **92**, 704–708.
- Sun, B. M., and P. Ya. Groisman, 2000: Cloudiness variations over the former Soviet Union. *Int. J. Climatol.*, **20**, 1097–1111.
- Trenberth, K. E., and J. T. Fasullo, 2009: Global warming due to increasing absorbed solar radiation. *Geophys. Res. Lett.*, **36**, L07706, doi:10.1029/2009GL037527.
- Wang, B., and Z. Fan, 1999: Choice of South Asian summer monsoon indices. *Bull. Amer. Meteor. Soc.*, **80**, 629–638.
- , R. Wu, and K.-M. Lau, 2001: Interannual variability of Asian summer monsoon: Contrast between the Indian and western North Pacific–East Asian monsoons. *J. Climate*, **14**, 4073–4090.
- Warren, S. G., and C. J. Hahn, 2002: Cloud climatology. *Encyclopedia of Atmospheric Sciences*, J. R. Holton, J. Pyle, and J. A. Curry, Eds., Oxford University Press, 476–483.
- , —, J. London, R. M. Chervin, and R. L. Jenne, 1986: Global distribution of total cloud cover and cloud type

- amounts over land. NCAR Tech. NCAR/TN-273+STR, 229 pp.
- , R. Eastman, and C. J. Hahn, 2007: A survey of changes in cloud cover and cloud types over land from surface observations, 1971–1996. *J. Climate*, **20**, 717–738.
- WMO, 1974: Manual on codes. Vol. 1. World Meteorological Organization Publ. 306, 348 pp.
- Wylie, D., D. L. Jackson, W. P. Menzel, and J. J. Bates, 2005: Trends in global cloud cover in two decades of HIRS observations. *J. Climate*, **18**, 3021–3031.
- Xia, X., 2012: Significant decreasing cloud cover during 1954–2005 due to more clear-sky days and less overcast days in China and its relation to aerosol. *Ann. Geophys.*, **30**, 573–582.
- Yin, J. H., 2005: A consistent poleward shift of the storm tracks in simulations of 21st century climate. *Geophys. Res. Lett.*, **32**, L18701, doi:10.1029/2005GL023684.
- Zhao, P., S. Yang, and R. Yu, 2010: Long-term changes in rainfall over eastern China and large-scale atmospheric circulation associated with recent global warming. *J. Climate*, **23**, 1544–1562.